Photochemical & Photobiological Sciences

PAPER

Cite this: *Photochem. Photobiol. Sci.*, 2018, **17**, 221

Lanthanide complexes of spiropyran photoswitch and sensor: spectroscopic investigations and computational modelling

M. S. A. Abdel-Mottaleb, *[a] M. Saif,[b] M. S. Attia,[a] M. M. Abo-Aly[a] and Sarah N. Mobarez [a]

Received 17th June 2017,
Accepted 22nd December 2017

DOI: 10.1039/c7pp00226b

rsc.li/pps

A number of novel lanthanide (Gd^{3+}, Sm^{3+}, and Tb^{3+}) complexes of the 1′,3′-dihydro-8-methoxy-1′,3′,3′-trimethyl-6-nitrospiro[2*H*-1-benzopyran-2,2′-(2*H*)-indole] (spiropyran; SP), a widely studied molecular photoswitch, were investigated. Comparative spectroscopic (absorption and fluorescence) and kinetic investigations of the stimulated photochromic and solvatochromic behavior were carried out in different media. SP embedded in a rigid thin film of poly(methylmethacrylate) might be exploited profitably as an optical sensor for the identification of a solvent's nature. Furthermore, thermodynamic parameters, in particular, Gibbs' free energy change ($\Delta G°$), were derived using density functional theory quantum chemical calculations with the SP and merocyanine coloured form. The model used was the B3LYP/6-31G(d,p)/SCRF = (SMD, solvent) and its time-dependent extension procedure was used to quantitatively explain the structural isomerization in response to a variety of stimuli, such as light, solvent nature, lanthanide(III) ions, and macromolecular support. These findings might be useful for the design of photoswitchable and energy transfer materials and their related fields.

1. Introduction

Spiropyrans[1] (SPs) are the core of the most widely studied class of organic photochromism. What makes SPs unique among the broad spectrum of photoswitches such as azobenzenes, stilbenes, diarylethenes, and fulgides, however, is that its two isomers (see Scheme 1) have different properties. As a consequence, many authors considered SP to be far more than just a simple photoswitch. The wide range of factors able to induce its reversible isomerization includes different solvents, metal ions, acids and bases, among others. However, the exact mechanism of photocoloration has yet to be determined.[2–7]

In general, SP is stable in its closed-ring isomeric form, and is a colourless or pale yellow solution in non-polar solvents. Ultraviolet (UV) irradiation of this SP form induces conversion to a coloured open-ring isomer (merocyanine; MC), which exhibits an absorption peak at 550–610 nm. The original colourless SP form can be restored by visible light irradiation and/or thermal induction. The mechanism by which the photochromism occurs is actually rupture of the C_{spiro}–O bond, induced by the UV irradiation. The result is a ring-opened coloured species, Scheme 1, which can be a *cis*-, *trans*- or *ortho*-quinoidal form. The introduction of the nitro chromogenic group into the benzene ring of the chromene part of the SP, which acts as a π-accepting substituent,[8] leads to a strong red shift in the MC isomer.[9–11] Spiropyrans in their closed form are soluble in a wide range of organic solvents and display quite low water solubility.[12] The doping of the SP in a rigid matrix such as poly(methylmethacrylate) (PMMA) or tetraethoxysilane gives the SP new properties which are very important in applications involving optical recording data, and sensors.[13–15] Spiropyrans with metal ion complexes have been used for recording optical data and increase the length of time of its storage.[16–21] They are also used as photochromic lenses.[22–26] Klajn reviewed SP-based dynamic materials[2] and showed that the SP and MC spectroscopic properties are linked to its responsiveness to different stimuli. In addition to being photochromic, its reversible isomerization can be achieved using some other independent stimuli, which include temperature (thermochromism), pH (acidochromism), solvent polarity (solvatochromism), redox potential (electrochromism), metal ions, and even mechanical force (mechanochromism). It has been concluded that the use of the SP switch would undoubtedly enable these materials to be used in far-reaching applications in the near future.[1]

[a]*Nano/Photochemistry, Solar Chemistry and Computational Chemistry Labs, Department of Chemistry, Faculty of Science, Ain Shams University, 11566 Abbassia, Cairo, Egypt. E-mail: m.s.abdelmottaleb@sci.asu.edu.eg*
[b]*Department of Chemistry, Faculty of Education, Ain Shams University, Roxy 11711, Heliopolis, Cairo, Egypt*

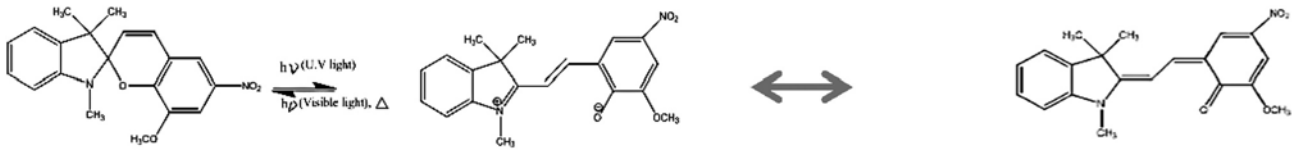

Scheme 1 Closed and open forms of the spiropyran studied and the resonance between the zwitterionic and quinoidal MC forms.

Piard[6] presents a paper, which is based on original results published elsewhere about the reaction shown in Scheme 1 and Rzepa[7] investigated the reaction path of this transformation using quantum chemistry.

Previous studies show that ring opening involving the spiro$_{C-O}$ bond rupture, with a *Z*/*E* isomerism of the alkene (concurrent or consecutive) occurs (see for example ref. 2 and 27). However, a crystal structure study of a dinitro analogue reveals the establishment of the trans (Entgegen) stereochemistry.[28] The zwitterion produced is highly coloured (blue-purple) unlike the colourless reactant. The rate at which this colour fades can be easily followed spectrophotometrically, and from these activation parameters the rate can be inferred as a function of the solvent.[7]

All the previously mentioned properties of SPs inspired the research reported in this paper on kinetic studies of UV irradiation/dark reactions and particularly the effect of complexation with different lanthanide cations such as gadolinium (Gd^{3+}), samarium (Sm^{3+}), and terbium (Tb^{3+}) on the spectroscopic properties of 1′,3′-dihydro-8-methoxy-1′,3′,3′-trimethyl-6-nitrospiro[2*H*-1-benzopyran-2,2′-(2*H*)-indole]. As far as is known, the influence of these specific lanthanide ions on the photochromic reaction of SP has never been published before. Furthermore, in order for this dynamic material to be robust and ultimately meet the requirements of real-world applications, it is necessary for such active components of the SP units to be embedded in the support. Thus, the study also explored embedding the SP in a rigid medium of a PMMA matrix. Furthermore, specific interactions in different media were also investigated. Additionally, supportive thermodynamics data derived from density functional theory (DFT) quantum chemical calculations were used within the B3LYP/6-31G(d,p)/SCRF = (SMD, solvent) procedure[29–32] to test the solvent influence on the MC → SP back reaction. Fig. 1 depicts the forms of the SP (form a) and MC (*Z* form b and *E* form c).

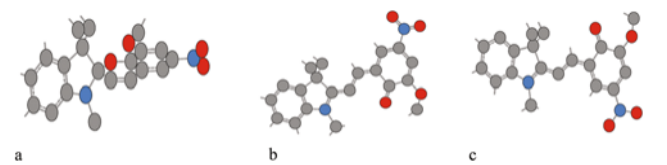

Fig. 1 SP and MC forms studied (a – closed SP form, b – MCTC (reported previously as TTC[27]) isomer and c – MCTT (reported previously as TTT[27] isomer)).

Further supportive computed quantitative molecular descriptors, particularly for the MC isomer in different solvents and of the Sm(III) complex, as a representative example of lanthanides, were computed and analysed. Computed fluorescence data is also reported and discussed.

2. Experimental

2.1. Materials

The SP (1′,3′-dihydro-8-methoxy-1′,3′,3′-trimethyl-6-nitrospiro[2*H*-1-benzopyran-2,2′-(2*H*)-indole]) (97%, Sigma-Aldrich) was used as received. Pure grade solvents (Sigma-Aldrich) were used. The lanthanide metal nitrates (Gd^{3+}, Sm^{3+}, and Tb^{3+}; 99.99%, Sigma-Aldrich), methylmethacrylate (MMA) and PMMA were used as received.

2.1.1 Preparation of spiropyran solutions. All the working solutions (5.0×10^{-5} mol L^{-1}) were prepared by taking 0.1 mL from the toluene stock solution (5.0×10^{-3} mol L^{-1}) and the solution was made up to 10 mL using solvent, and thus, the working solution contains 1.0% toluene. The lanthanide metal nitrates were used as received and all the working solutions (5.0×10^{-5} mol L^{-1}) of these contained 1% of absolute ethanol (Et). The solutions of the complexes were prepared by mixing a metal nitrate with SP in a molar ratio of 1 : 1 in different solvents.

2.1.2 Preparation of spiropyran doped in a PMMA matrix. The PMMA matrix was prepared by dissolving 5 g of PMMA in 25 mL of toluene at 25 °C with vigorous stirring for 15 min, then 0.25 mL of 5.0×10^{-3} mol L^{-1} of SP was added to the PMMA solution with stirring for 15 min. The solution was poured into a Petri dish and the PMMA matrix was left to dry for two days at room temperature to obtain the PMMA thin film (SP concentration is 5.0×10^{-5} mol L^{-1}).[33,34]

2.2. Instruments

Ultraviolet-Visible (UV-Vis) absorption spectra were measured in the range of 250–800 nm using an Ocean Optics diode array spectrophotometer with SpectraSuite operating software. The source of the UV irradiation was a homemade photoirradiation apparatus with an 8 W UVA lamp. The fluorescence spectra of the prepared samples were obtained using a PerkinElmer LS 55 luminescence spectrometer.

2.3. Kinetics measurements

The kinetic rate parameters of the colour developing reaction [MC] and the back reaction of [SP] follow first order kinetics.

The integrated form of the first-order rate law for the photocoloration process is given as:

$$\ln([A_{MC}]_t - [A_{MC}]_{eq.}) = -k_{obs}t + \ln([A_{MC}]_0 - [A_{MC}]_{eq.})$$

where k_{obs} is the rate constant, and $[A_{MC}]_{eq.}$, $[A_{MC}]_t$ and $[A_{MC}]_0$ are the absorbances of the MC at infinite time, at time t, and at zero time, respectively.[23] The plot of $\ln([A_{MC}]_t - [A_{MC}]_{eq.})$ against the irradiation time gives a straight line with slope which equals k_{obs}.

2.4. Computations

Computations were carried out using the Gaussian 16 (Revision A.03) software[35] and the Spartan'16 Parallel Suite QC program (Spartan'16 version 2.0.3, Wavefunction, Inc., USA).[36] For this research, the B3LYP/6-31G(d,p) model was used. Spartan'16 was used to obtain the electrostatic potential (ESP) maps, the ionization potential (IP) maps and the structure descriptors.

Extensive singlet-state emission computations were carried out by computing the potential energy surface (PES) of the excited state. The lowest energy predicted for the optimized excited state structure corresponds to the energy emitted when the molecule fluoresces as it deactivates and goes back to the ground state. The ground state of the closed and open forms were first optimized, followed by time-dependent density functional theory (TD-DFT) calculations using the CAM-B3LYP/6-31G9(d,p) model and SCRF = (CPCM, toluene or ethanol). The state was then optimized at the largest oscillator strength, which was the 4th and the 1st excited states for SP and its open MCTT structures, respectively. The optimized structures of the isomers in both states were not significantly changed.

Thermodynamic parameters, especially the Gibbs' free energy, derived from quantum chemical calculations with MC were used within the B3LYP/6-31G(d,p)/SCRF = (SMD, solvent) procedure[37] to test the solvent influence on the back reaction.

3. Results and discussion

3.1. Modelling of photochromism

It was established that the possibility for the SP compound to exhibit photochromic properties is related to ring opening through spiro$_{C7-O13}$ bond rupture followed by change of the dihedral angle between C7, C12, C15, C17, to form the most stable coloured *E* isomer. These calculations demonstrate these processes by using the relative energy profiles because the bond rupture and dihedral angle change shown in Fig. 2 reveal this model. Obviously, C–O bond rupture leads to destabilization of the SP total energy, which regains its stabilization from isomerization *via* a dihedral angle change from −9° to 180° (*E* isomer). Increasing the distance of C–O from 1.44 Å to 2.33 Å results in destabilization of the open form, then a minimum energy is achieved at 2.77 Å. Further increase in C–O distance increases the molecular energy again. To achieve molecular stability, the molecule changes its orientation by changing the dihedral angle across a barrier of about 22 kcal mol^{-1} to gain the relatively stable orientation of the *E* isomer.

3.2. Absorption spectra and solvent effect

The absorption spectrum of the SP in absolute ethanol shows three bands at 288 nm, 359 nm and 574 nm. The two bands at 288 nm and 359 nm are attributed to π–π* transitions in the closed form. The band at 574 nm is attributed to the formation of the more conjugated open form (MC) (see Fig. 3). Light-induced ring opening is shown in Fig. 3B.

In complete agreement with the previously reported results, polar protic and aprotic solvents have stimulant effects on SP ring opening in the dark (Table 1) because of the stabilization

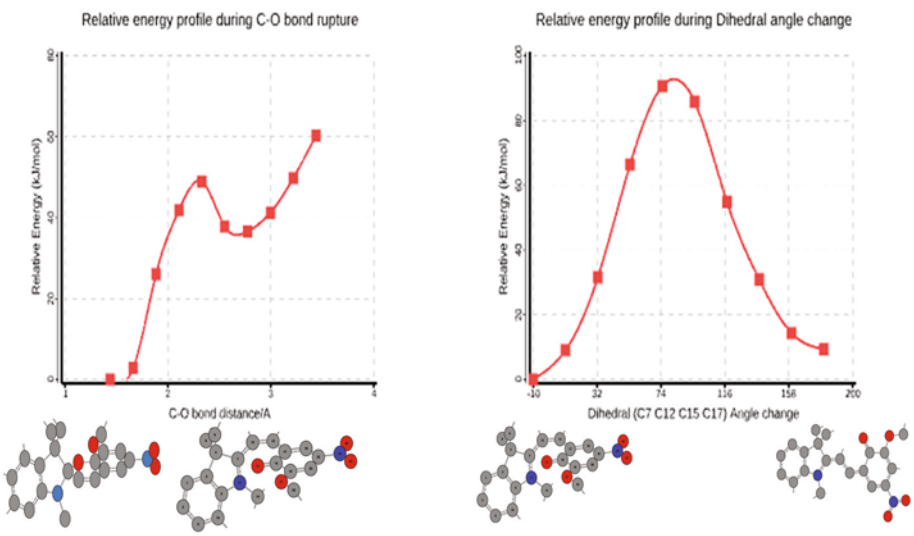

Fig. 2 Relative energy profiles of spiro$_{C-O}$ bond rupture and dihedral angle change responsible for coloured appearance because of the SP-MCTT transformation (computed with Spartan'16 Parallel Suite program).

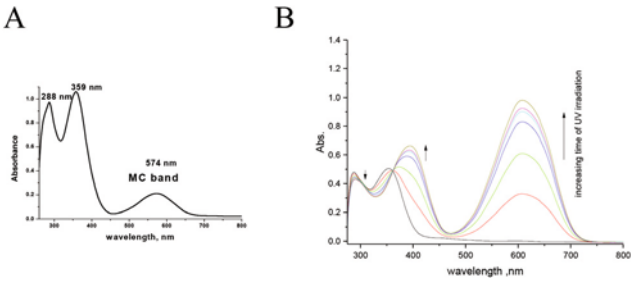

Fig. 3 (A) Absorption spectrum of SP in ethanol showing partial formation of the MC form. (B) Colour development by irradiation of SP in toluene.

of the zwitterionic form even in the dark.[2] This can be further explained using DFT computations, which have recently been published, and which reveals that the electron-withdrawing NO_2 group of the benzopyran part is significantly lower than the C–O cleavage activation energy and accelerates the SP/MC isomerization even in the dark.[2c] The equilibrium ratio between SP and MC in solution is dictated by the hydrogen bonding donor ability (α value) of the solvent[38] generating a hydrogen bonded adduct SP-HOEt, which facilitates C_{spiro}–O bond rupture, and the equilibrium is shifted more to the coloured MC form that partially appears in the ground state (see Fig. 2).

Because of its planar structure and an extended π-conjugation between the indoline and the chromene moieties, MC shows a single delocalized transition in the visible region, with λ_a = 552–612 nm in different solvents (see Table 1). The exact location of this band is dictated by the relative contributions of the two extreme resonance forms. The strong dependence of MC absorption on the environment suggests that it could be exploited as the solvent's sensor (see section 3.6).

As expected, the data in Table 1 show that the half-life ($t_{1/2}$, s) and the rate of dark reaction (k_2 value) of the open form of MC reveal that there is stabilization in the polar solvents as also reflected in the higher values of k_1 relative to k_2. The high π value together with noticeable high H-bonding donor and acceptor (α and β) values of these solvents may synergistically act together resulting in the remarkable stabilizing solvation process of the dipolar MC form. Non-polar solvents favour conversion to the SP form as indicated by the remarkable enhancement of the k_2 value and the small half-life of the MC. The rate of the forward reaction (k_1) to produce MC confirms this process (see Table 1).

In a mixed solvent system of a non-polar solvent and a polar solvent [1,4-dioxane and water (H_2O), it was noticed that by increasing the percentage of water from 0% to 50% the back reaction slowed down and the rate constant decreased from 1.6×10^{-2} s^{-1} in 100% dioxane solution to 10^{-4} s^{-1} in a 50% dioxane + 50% water system (see Table 2 and Fig. 4). The MC stabilization reached its maximum in the 50% dioxane + 50% water system and the half-life of MC was 20 times greater than that in pure dioxane solvent. Furthermore, the λ_{MC} peak was blue shifted with increasing medium polarity.

Thermodynamic parameters, derived from quantum chemical calculations with MC were used within the B3LYP/6-31G(d, p)/SCRF = SMD, solvent procedure, which had been recommended before by previous researchers,[36] to test the solvent influence on the back reaction. Thermodynamic data are collected in Tables 3–5.

The next section discusses the effect of solvent in terms of the computed thermodynamics. Most remarkable are those of

Table 2 Effect of increasing percentage of water in the mixed solvent system of 1,4-dioxane and water on the rate constants of the colour developing and back reactions, MC half-life and MC maximum wavelength (SP concentration = 5×10^{-5} M).[a]

% Dioxane/H_2O (v/v)	$k_1 \times 10^3$ (s^{-1})	$k_2 \times 10^4$ (s^{-1})	$t_{1/2}$ (s)	λ_{MC} (nm)
100/0	24.0	160.0	40	603
90/10	20.0	100.0	45	573
80/20	7.6	32.0	110	566
70/30	5.2	12.0	230	560
60/40	3.8	3.4	390	555
50/50	2.7	1.0	800	551

[a] k_1., k_2: the rate constants of the colour developing and dark reactions, respectively. $t_{1/2}$: the half-life of the MC form and λ_{MC}: the maximum wavelength of the MC form.

Table 1 Solvent and kinetic parameters of the MC form in different media (of variable microscopic solvent polarity parameters[38])

Solvent[a]	α	β	π	$t_{1/2}$ (s)	$k_1 \times 10^3$ (s^{-1})	$k_2 \times 10^3$ (s^{-1})	λ_{MC} (nm)
Methanol	0.93	0.62	0.6	80	8	2.5	552
Ethanol	0.83	0.77	0.54	160	12	2.5	564
DMSO	0	0.76	1	118	12	1.7	553
DMF	0	0.69	0.88	80	8.5	5.6	584
1,4-Dioxane	0	0.37	0.55	40	24	16.0	604
Benzene	0	0.10	0.59	35	38	22.0	612
Toluene	0	0.11	0.54	40	34	16.0	609

[a] Where α is the solvent hydrogen bond-donor ability (α-HBD acidity), β is the solvent hydrogen bond-acceptor ability (β-HBD acidity), and π is the solvent polarity. α, β, and π are microscopic solvent polarity parameters. $t_{1/2}$ is the half-life of the MC form (the time taken by the MC maximum absorbance to fall to its half value), k_1 and k_2 are the initial rate constants of the forward and dark reactions, respectively, and λ_{MC} is the maximum wavelength of MC (SP concentration = 5×10^{-5} M). DMF: dimethylformamide, DMSO: dimethylsulfoxide.

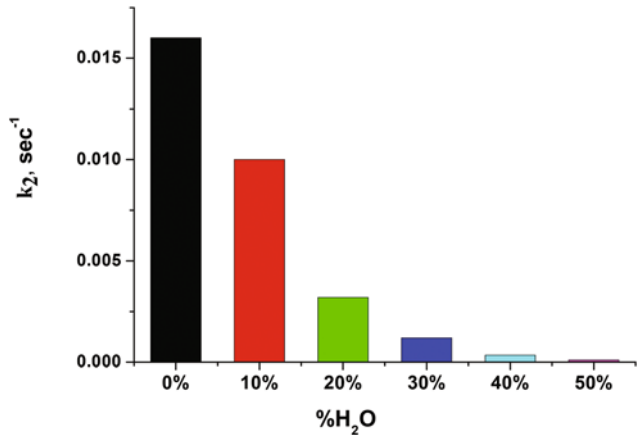

Fig. 4 Effect of increasing H_2O content (%, v/v) in 1,4-dioxane/H_2O mixtures on the initial rate constant of the back reaction (k_2).

the activation parameters for the thermal back reaction. Continuing from the gaseous phase to toluene, the calculated activation entropy ΔS changes with solvent by around 4 cal K^{-1} mol^{-1} and 3 cal K^{-1} mol^{-1} for MCTC and MCTT, respectively. The enthalpy changes are pronounced (ΔH changes by about 7 kcal mol^{-1}) for EtOH because of the hydrogen bonding effect (see Tables 3 and 5). Less positive ΔH and ΔG values in toluene favour the SP form, whereas a larger value points to ring opening in dark forming, coloured MC, preferably MCTC in EtOH. Table 4 summarizes some descriptors of molecular properties of the MC (MCTC) isomer in different media. The nature of the medium has a negligible effect on the value of the space filling model (space-filling calotte models are also referred to as CPK models after the chemists Robert Corey, Linus Pauling, and Walter Koltun) area and volume of the molecule as well as its polarizability. However, $\Delta G^{\circ}_{solvation}$ and dipole moment show much sensitivity towards the nature of the medium (see Table 4). Generally, polarizability increases as the volume occupied by the electrons increases as in the case of the Sm(III) complex, which reflects the diffusiveness of the electronic charge induced by the lanthanide ion. In other words, larger molecules are generally more polarizable than the smaller ones.

More detailed discussion on the thermodynamic data change because of the complexation with lanthanides (Table 4) is discussed in the following section.

3.3. Effect of metal complexation on SP/MC ratio in solution

Ring opening is stimulated by presence of lanthanide ions as has been previously reported.[33,40] The influence of the lanthanide metal ions, Gd^{3+}, Sm^{3+}, and Tb^{3+} on the photochromic reaction of this molecule has never been published before. It is obvious that successive addition of lanthanide metal ions turns the colourless solution of the SP into a red coloured solution (colourless → red) (Fig. 5). This is because the complex formation between the MC, which could act as a bidentate ligand, and the lanthanide ions in the solution. This

Table 3 Computed thermodynamic parameters for the optimized SP and its most stable optimized open isomers using the G(d,p) basis set)/Gaussian 09 computations[a]

	$G^{\circ}_{298.15}$ (Hartree)			H° (Hartree)			S (cal K^{-1} mol^{-1})		
Solvent	SP	MCTC	MCTT	SP	MCTC	MCTT	SP	MCTC	MCTT
Gas	−1184.164068	−1184.163783	−1184.163187	−1184.088439	−1184.083271	−1184.081784	+159.175	+169.453	+171.326
EtOH	−1184.186015	−1184.197503	−1184.196656	−1184.110665	−1184.117654	−1184.116799	+158.587	+168.057	+168.074
DMSO	−1184.182820	−1184.191164	−1184.191259	−1184.107004	−1184.109246	−1184.111395	+159.567	+167.214	+168.087
Toluene	−1184.185010	−1184.188695	−1184.187887	−1184.109289	−1184.112367	−1184.107844	+159.368	+165.842	+168.465

[a] 1 Hartree = 2625.5 kJ mol^{-1} or = 627.5 kcal mol^{-1}.

Table 4 Effect of medium and metal ions on some molecular structure descriptors computed using the Spartan'16 Parallel Suite (with the G+31 basis set)

Label	E_{HOMO} (eV)	E_{LUMO} (eV)	Dipole (Debye)	CPK area (Å^2)	CPK volume (Å^3)	Polarizability	$H°$ (Hartree)	$G°$ (Hartree)
Vacuum	−5.29	−2.72	12.64	373.25	359.01	69.89	−1184.05721	−1184.12437
EtOH	−5.47	−2.67	21.06	374.1	359.3	69.86	−1184.09291	−1184.16015
DMF	−5.22	−2.47	19.69	373.68	359.12	69.86	−1184.09064	−1184.15778
Toluene	−5.23	−2.6	15.81	373.4	359.02	69.88	−1184.08353	−1184.15066
Sm(III)	−14.2	−13.59	16.57	391.84	373.6	71.54	−1220.23871	−1220.30955

$\Delta G^{\circ}_{solvation} = 22.47, 20.99$ and 16.51 kcal mol^{-1} for EtOH, DMF and toluene, respectively. Sm(III) induced a tremendous stability gain of −36.18518 au relative to MCTC in vacuum. $G_{solvation}$ is the change in energy because of the transfer of a molecule from the gas phase to solution.[39] The HOMO–LUMO gap is smallest in the presence of Sm(III) and increases, as expected, in the order vacuum (2.59) < toluene (2.63) < DMF (2.75) < EtOH (2.80). Molecular polarity also increases with solvent polarity.

Table 5 Computed activation parameters for the thermal back reaction/Gaussian 09 results

	$\Delta G^{\circ}_{298.15}$ (kcal mol^{-1})		$\Delta H°$ (kcal mol^{-1})		ΔS (cal K^{-1} mol^{-1})	
Solvent	SP-MCTC	SP-MCTT	SP-MCTC	SP-MCTT	SP-MCTC	SP-MCTT
Vacuum	−1.788	−0.553	−3.246	−4.180	−10.278	−12.151
EtOH	+7.209	+6.677	+4.390	+3.853	−9.470	−9.487
DMSO	+5.236	+5.295	+1.408	+2.758	−7.647	−8.520
Toluene	+2.312	+1.805	+1.933	−0.908	−6.474	−9.097

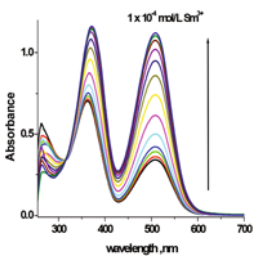

Fig. 5 Absorption spectra of 5.0 × 10^{-5} mol L^{-1} SP in 1,4-dioxane after addition of 1.0 × 10^{-4} mol L^{-1} Sm^{3+} at different time intervals: 0, 2, 6, 12, 25, 55, 100, 160, 235, 325, 430, 550 and 835 s.

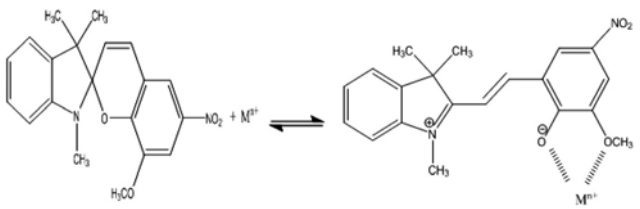

Scheme 2 Complex formation after the addition of the metal ion to the SP solution.

is quite understandable because the presence of a methoxy group at the *ortho* position to the phenolate oxygen leads to remarkable stabilization of the MC (see Table 5 and Scheme 2). TD-DFT calculations of the open form of the SP complex show that the main transitions are at 510 nm (mainly HOMO → LUMO) and at 370 nm (mainly HOMO−1 → LUMO transition), which overlaps with the HOMO → LUMO+1 transition of the closed SP form which appears at 370 nm. This is reflected in the enhancement of both absorption bands by the addition of lanthanide ions. Furthermore, the MC peak is blue shifted by approximately 100 nm after the addition of Gd^{3+}, Sm^{3+}, and Tb^{3+} ions. These ions strongly stabilize the MCTC form (see Table 4). For example, Sm(III) induced a tremendous thermodynamic stability gain $\Delta G°$ = −36.18518 au relative to MCTC in vacuum (Table 4). This was verified experimentally by the remarkable decrease of the rate of the dark reaction (k_2 value; Fig. 6).

Additional theoretically computed molecular descriptors are summarized in Table 4 and some important surface properties of the MCTC-Sm(III) complex are shown in Fig. 7. The relationships between the properties or descriptors are of interest. For example, the difference in the HOMO and LUMO energies (the HOMO–LUMO gap) is of interest: electronegativity or the chemical potential descriptor: (HOMO + LUMO)/2 (eV) and hardness descriptor: (HOMO–LUMO)/2 (eV), which measure the escape tendency of electrons or the resis-

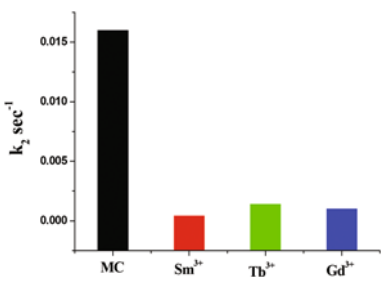

Fig. 6 Effect of the lanthanides (Gd^{3+}, Sm^{3+}, and Tb^{3+}) addition on the initial rate constant of the back reaction (k_2) (SP concentration = 5.0 × 10^{-5} mol L^{-1}, lanthanide metal concentration = 5.0 × 10^{-5} mol L^{-1}).

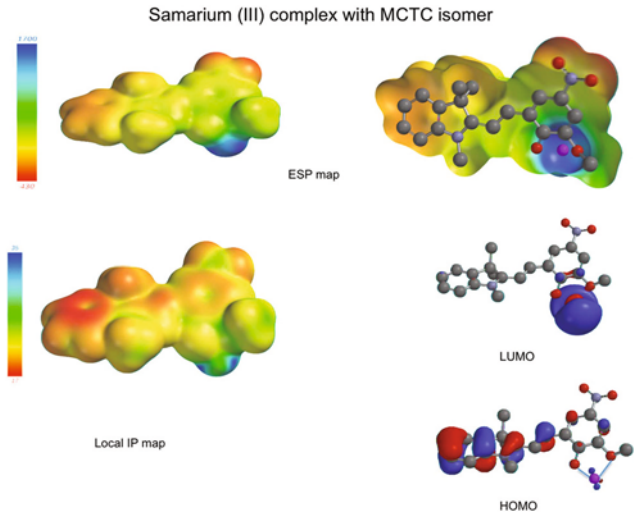

Fig. 7 Computed surfaces of MCTC-Sm(III) complex using Spartan'16 Parallel Suite program showing some reactivity maps and surfaces. LUMO is mainly localized on the Sm(III)-bidentate oxygens of the MCTC whereas the HOMO is mainly localized on the indoline part of the SP reflecting the ligand-to-metal charge transfer nature of the longest wavelength transition.

tance to charge transfer, respectively.[41] Table 4 shows clearly the solvent and metal ion induced changes in these molecular properties. Similar results were obtained for the other lanthanide ions. The ESP map and the local IP map reflect the large nucleophilic character of such a complex. A more interesting observation is that for the longest wavelengths, electronic transition [from HOMO, mainly localized on the indoline part of the molecule, to LUMO, which is mainly localized on the Sm(III)] could be assigned as a ligand for metal charge transfer transition (L-to-MCT).

3.4. SP-PMMA matrix

Incorporation of a SP-MC molecular switch onto the macromolecular supports allows for the creation of materials which are easy to handle. The λ_{max} of the MC form is blue shifted by 11 nm in the PMMA matrix compared to in toluene (Table 1). The coloration rate constant in the SP-PMMA matrix equals 5.5×10^{-3} s^{-1} whereas, in the MMA monomer, it equals 0.12 s^{-1}. The discoloration rate constant for SP embedded in PMMA film is 77 times smaller than the rate of discolouration of MC in the MMA monomer (Fig. 8 and Table 1). These values were attributed to the steric hindrance and the small free volume present between the polymer chains. SP with the two perpendicular fragments occupies a smaller volume than the MC form with the planar structure, so it is difficult for the SP → MC transformation to proceed. Also, it is difficult for the *trans* MC form produced to rotate and return back to the closed SP form. This confirms that the half-life of the MC form in the polymer film is higher than in the MMA monomer (see Table 1).

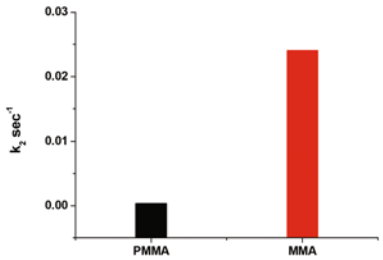

Fig. 8 A graphical representation showing the rigidity effect on the initial rate constant of the back reaction, MC → SP (k_{obs}).

3.5. UV irradiation and relaxation

Upon UV irradiation, the absorbance of both the MC form at 610 nm and the MC-M^{3+} complexes at 509 nm increases with increase in the UV irradiation time and the absorbance of the closed SP form decreases. In the dark reaction negative photochromism takes place and the absorbance of MC decreases as shown in Fig. 9 and 10. It is interesting to note that in all the absorption spectra recorded, a clear isosbestic point is seen in all the media as well with lanthanide ion addition, and this indicates the establishment of equilibrium between the open and the closed forms of the photochromic material under investigation.

3.6. Photoluminescence properties

To test the potential of the SPs as sensitizers for energy transfer to the lanthanide ions (Gd^{3+}, Sm^{3+}, or Tb^{3+}), some photoluminescent (PL) measurements were carried out and these are reported here. Fig. 11 shows the excitation and emission spectra of SP in toluene before and after 50 min of UV illumi-

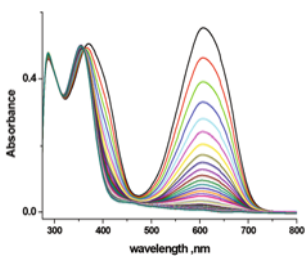

Fig. 9 The decrease in the absorption spectrum of 5×10^{-5} M solution of previously irradiated SP in toluene at 10 s intervals during the dark reaction (colour fading in the dark).

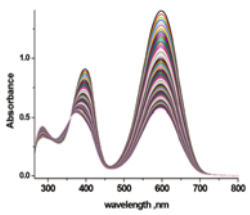

Fig. 10 The absorbance decrease in the absorption spectrum of previously irradiated SP–PMMA film every 40 s during the dark reaction.

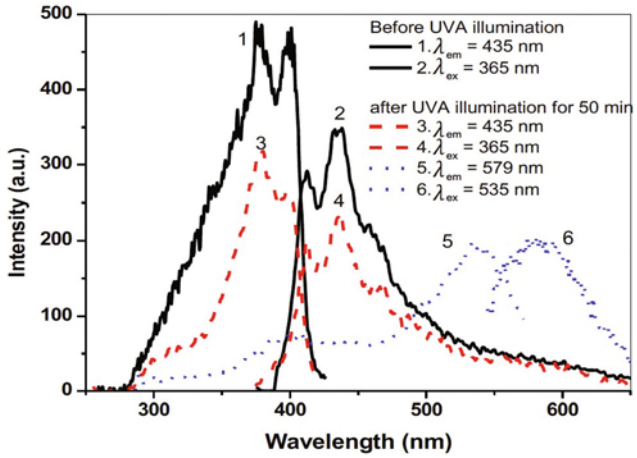

Fig. 11 The excitation and emission spectra of SP and MCTT isomers in toluene before and after UV illumination for 50 min. Computed values are given in Table 7.

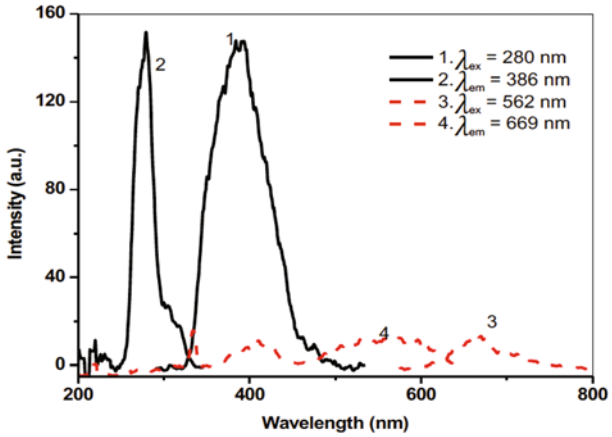

Fig. 12 The excitation and emission spectra of SP and MCTT isomers in ethanol.

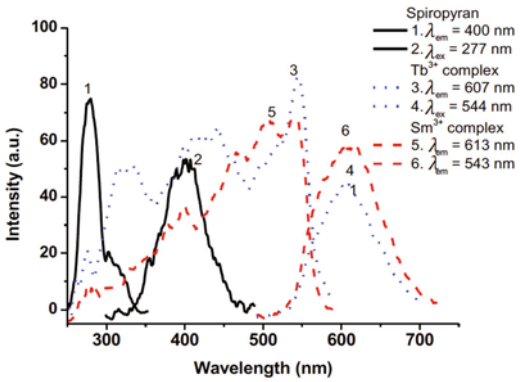

Fig. 13 The excitation and emission spectra of spiropyran and its lanthanide complexes in acetonitrile.

nation (curves 1 and 2). Before illumination, a violet PL emission (435 nm) was observed. Illumination of SP decreases the emission and excitation spectra centred at 435 nm and 365 nm, respectively (Fig. 11 (curves 3 and 4)). Also, the illuminated sample shows a new orange emission at 579 nm (dotted blue curve 6) and an excitation band with a maximum at 535 nm (dotted blue curve 5), which could be attributed to the generation of the MCTT-form of SP by the UV illumination.[42]

In a polar-protic solvent such as EtOH, a purple solution was obtained in dark conditions. This solution gave excitation bands in the UV (280 nm) and in the visible (406–562 nm) regions (Table 6). This confirms the presence of closed SP and open MC forms in EtOH. The closed SP form gives a strong emission band at 386 nm. Weak fluorescence of the MCTT at 669 nm in EtOH was obtained (Fig. 12). This is because of the favourable radiationless deactivation of its singlet state from the extensive torsional motions of this isomer. Furthermore, good agreement between experimentally measured fluorescence/excitation spectra and the calculated ones were obtained.

Spiropyran in acetonitrile gave a faint yellow solution, which displayed limited visible excitation (maximum excitation 277 nm) (Table 6). This solution shows a broad emission band in UVA region, which confirms the presence of a fluorescent closed SP form (Fig. 13). Upon complexation with Sm^{3+} or Tb^{3+} ions in the dark, the solutions became orange and the excitation spectra were red shifted (544 nm and 543 nm) in comparison with SP in the same solvent. The Sm^{3+} and Tb^{3+} complexes show broad red emission bands, which were consistent with MC formation and concomitant metal chelation (Fig. 13).

Because the radiationless deactivation channels (torsional motions around single bonds and isomerization around the double bonds) are closed in the SP form, it exhibits more enhanced fluorescence than its open flexible structure forms. Complexation with lanthanide ions induced fluorescence enhancement of the open coloured forms. Furthermore, no characteristic Sm^{3+} and Tb^{3+} emission bands were observed under spiropyran excitation in different solvents such as acetonitrile, DMF, ethanol and toluene. This means that the energy transfer probability is very low when using SP as a sensitizer.

The computed fluorescence maxima were in good agreement with the experimental values listed in Table 7. The data in Table 7 reveal that specific H-bonding interactions of the ethanol induce a significant decrease in the fluorescence maxima of both the closed and the open forms of the photochromic material.

Table 6 PL properties of SP and its lanthanide complexes in different solvents

Compound	Excitation wavelength (nm)	Emission wavelength (nm)
Spiropyran		
Toluene	365	435
Acetonitrile	277	400
EtOH	280, 406, 562	386, 669
Complex of Tb^{3+}		
Acetonitrile	544	607
Complex of Sm^{3+}		
Acetonitrile	543	613

Table 7 Computed fluorescence spectra of the SP and its MCTT isomer in different media

Solvent	SP form λ (nm (f))	MCTT form λ (nm (f))
EtOH	527.84 (0) dark transition	559.26 (0.5586)
Toluene	549.15 (0) dark transition	616.03 (0.5043)
Gas	550.25 (0.0010)	617.31 (0.3468)

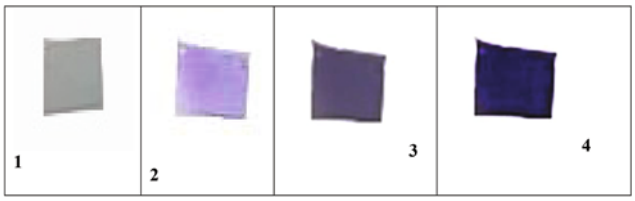

Fig. 14 SP embedded in PMMA film (1) – before immersion in EtOH, and after immersion in EtOH for (2) – 30 min, (3) – 1 h and (4) – 2 h.

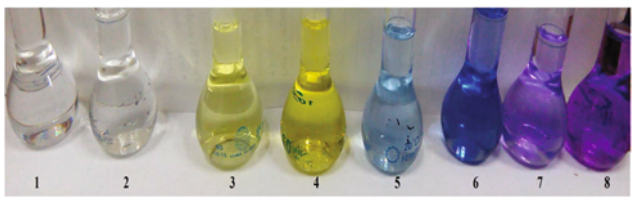

Fig. 15 Colour response of SP/MC from the solvent stimuli: 1 – toluene, 2 – 1,4-dioxane, 3 – acetonitrile, 4 – acetone, 5 – DMF, 6 – DMSO, 7 – EtOH, and 8 – methanol.

3.7. Application of SP embedded in PMMA film as a sensor for solvent polarity

The SP-PMMA film can be used as sensor for the identification of the solvents' polarity. After immersing the polymer film in EtOH it became coloured (colourless → violet) after 40 min and after 2 h the colour became deeper and the intensity of MC peak was remarkably enhanced. However, in solvents of different polarities, SP develops different colours (Fig. 14 and 15) because of the gradual increasing of ring opening to form MC. Furthermore, upon UV irradiation, if the MC isomers formed were dissolved in different solvents, they exhibited different colours. Both, the SP and MC isomers show solvatochromic behaviour as discussed previously.

4. Conclusions

The influence of lanthanide metal ions (Gd^{3+}, Sm^{3+}, or Tb^{3+}) on the photochromic reaction of this molecule has never been published before. The intensity of the absorption band of MC increases in the presence of these lanthanide metal ions. Photoluminescence results show that the probability of energy transfer to the lanthanide ions is very low when using SP as a sensitizer. Polar protic and aprotic solvents and lanthanide ions gave the expected stimulant effects on the SP ring opening in the dark because of the stabilization of the zwitterionic coloured open form. Positive photochromism takes place in non-polar solvents whereas negative photochromism occurred in polar solvents. In a mixed solvent (H_2O–dioxane) the increase of the water ratio up to 50% stabilizes the dipolar MC form. A thin film of SP material in the PMMA matrix could be successfully exploited as a sensor for solvents. Because the radiationless deactivation channels (torsional motions around single bonds and isomerization around the double bonds) is closed in the SP form, it exhibits more enhanced fluorescence than its open flexible structure forms. Complexation with lanthanide ions induced fluorescence enhancement of the open coloured forms. Complexation with lanthanide ions induced fluorescence enhancement of the open coloured forms probably because of the closing of the torsional channels of the binding sites that slowed down the rate of radiationless transitions. The effect of solvent nature in terms of the computed thermodynamics using DFT was determined. The most remarkable effects found were those relating to the activation parameters for the thermal back-reaction, such as $\Delta G°$, $\Delta H°$, and ΔS, which explain the SP/MC ratios obtained in different media and upon complexation with lanthanides. Additional supporting results for the computed surfaces of the MCTC-Sm(III) complex were presented in Fig. 7. It was found that LUMO was mainly localized on the Sm(III)-bidentate oxygens of the MCTC whereas the HOMO is mainly localized on the indoline part of the SP reflecting the ligand-to-metal charge transfer nature of the longest wavelength electronic transition. These findings might be useful in the design of energy transfer materials and in related fields.

Conflicts of interest

There are no conflicts to declare.

Notes and references

1 A. Mustafa, *Chem. Rev.*, 1948, **43**, 509–523.
2 (*a*) R. Klajn, *Chem. Soc. Rev.*, 2014, **43**, 148–184 and references cited therein. (*b*) S. Aiken, R. J. L. Edgar, C. D. Gabbutt, B. Mark Heron and P. A. Hobson, *Dyes Pigm.*, 2018, **149**, 92–121; (*c*) Pi.-X. Wang, Fu.-Q. Bai, Z.-X. Zhang, Y.-P. Wang, J. Wang and H.-X. Zhang, *Org. Electron.*, 2017, **45**, 33–41.
3 Y. Sheng, J. Leszczynski, A. A. Garcia, R. Rosario, D. Gust and J. Springer, *J. Phys. Chem. B*, 2004, **108**, 16233–16243.
4 S. Yagi, S. Nakamura, D. Watanabe and H. Nakazumi, *Dyes Pigm.*, 2009, **80**, 98–105.
5 A. Samoladas, D. Bikiaris, T. Zorba, K. M. Paraskevopoulos and A. Jannakoudakis, *Dyes Pigm.*, 2008, **76**, 386–393.
6 J. Piard, *J. Chem. Educ.*, 2014, **91**, 2105–2111 and references cited therein.

7 H. S. Rzepa, 2015 http://www.ch.imperial.ac.uk/rzepa/blog/?p=13300.
8 H. Görner, *Phys. Chem. Chem. Phys.*, 2001, **3**, 416–423.
9 D. Wang, P. Jiao, J. Wang, Q. Zhang, L. Feng and Z. Yang, *J. Appl. Polym. Sci.*, 2012, **125**, 870–875.
10 R. Byrne, C. Ventura, F. Benito Lopez, A. Walther, A. Heise and D. Diamond, *Biosens. Bioelectron.*, 2010, **26**, 1392–1398.
11 F. M. Raymo and S. Giordani, Signal processing at the molecular level, *J. Am. Chem. Soc.*, 2001, **123**, 4651–4465.
12 R. Rosario, D. Gust, M. Hayes, J. Springer and A. A. Garcia, *Langmuir*, 2003, **19**, 8801–8806.
13 A. K. Chibisov and H. Görner, *Chem. Phys.*, 1998, **237**, 425–442.
14 R. Heiligman-Rim, Y. Hirshberg and E. Fischer, *J. Phys. Chem.*, 1962, **66**, 2470–2477.
15 G. Berkovic, V. Krongauz and V. Weiss, *Chem. Rev.*, 2000, **100**, 1741–1754.
16 I. Willner, *Acc. Chem. Res.*, 1997, **30**, 347–356.
17 S. Kawata and Y. Kawata, *Chem. Rev.*, 2000, **100**, 1777–1788.
18 E.-Mi. Lee, S.-Y. Gwon, Y.-A. Son and S.-H. Kim, *Spectrochim. Acta, Part A*, 2012, **86**, 600–604.
19 F. Nourmohammadian and A. A. Abdi, *Spectrochim. Acta, Part A*, 2016, **153**, 53–62.
20 D. Y. Hur, T. J. Park and E. Ju. Shin, *Spectrochim. Acta, Part A*, 2014, **114**, 541–547.
21 A. O. Bulanov, L. D. Popov, I. N. Shcherbakov, V. A. Kogan, V. A. Barachevsky, V. V. Lukov, S. N. Borisenko and Yu. N. Tkachenko, *Spectrochim. Acta, Part A*, 2008, **71**, 1146–1152.
22 Photochromism, in *Techniques in Chemistry*, ed. R. C. Bertelson and G. H. Brown, Wiley-Interscience, New York, NY, USA, 1971, vol. 3, pp. 45–294.
23 S. V. Paramonov, V. Vladimir Lokshin and O. A. Fedorova, *J. Photochem. Photobiol., C*, 2011, **12**, 209–236.
24 J. Malkin, A. S. Dvornikov, K. D. Straub and P. M. Rentzepis, *Res. Chem. Intermed.*, 1993, **19**, 159–167.
25 R. F. Khairutdinov and J. K. Hurst, *Langmuir*, 2001, **17**, 6881–6886.
26 A. V. Chernyshev, N. A. Voloshin, A. V. Metelitsa, V. V. Tkachev, S. M. Aldoshin, E. Solov'eva, I. A. Rostovtseva and V. I. Minkin, *J. Photochem. Photobiol., A*, 2013, **265**, 1–9.
27 M. S. A. Abdel-Mottaleb and S. N. Ali, *Int. J. Photoenergy*, 2016, **2016**, 1–8.
28 J. Hobley, V. Malatesta, R. Millini, L. Montanari and W. O. Neil Parker Jr., *Phys. Chem. Chem. Phys.*, 1999, **1**, 3259–3267.
29 J. Ho and M. Z. Ertem, Calculating Free Energy Changes in Continuum Solvation Models, *J. Phys. Chem. B*, 2016, **120**, 1319–1329.
30 R. F. Ribeiro, A. V. Marenich, C. J. Cramer and D. G. Truhlar, *J. Phys. Chem. B*, 2011, **115**, 14556–14562.
31 A. V. Marenich, C. J. Cramer and D. G. Truhlar, *J. Phys. Chem. B*, 2009, **113**(18), 6378–6396.
32 J. H. Jensen, *Molecular Modelling Basics*, CRC Press, Taylor and Francis, NY, 2010, ch. 2, p. 72.
33 M. S. Attia, M. M. H. Khalil, M. S. A. Abdel-Mottaleb, M. B. Lukyanova, Yu. A. Alekseenko and B. Lukyanov, *Int. J. Photoenergy*, 2006, **2006**, 1–9.
34 A. Fissi, O. Pieroni, N. Angelini and F. Lenci, *Macromolecules*, 1999, **32**, 7116–7121.
35 M. J. Frisch, G. W. Trucks, H. B. Schlegel, G. E. Scuseria, M. A. Robb, J. R. Cheeseman, G. Scalmani, V. Barone, B. Mennucci, G. A. Petersson, H. Nakatsuji, M. Caricato, X. Li, H. P. Hratchian, A. F. Izmaylov, J. Bloino, G. Zheng, J. L. Sonnenberg, M. Hada, M. Ehara, K. Toyota, R. Fukuda, J. Hasegawa, M. Ishida, T. Nakajima, Y. Honda, O. Kitao, H. Nakai, T. Vreven, J. A. Montgomery Jr., J. E. Peralta, F. Ogliaro, M. Bearpark, J. J. Heyd, E. Brothers, K. N. Kudin, V. N. Staroverov, T. Keith, R. Kobayashi, J. Normand, K. Raghavachari, A. Rendell, J. C. Burant, S. S. Iyengar, J. Tomasi, M. Cossi, N. Rega, J. M. Millam, M. Klene, J. E. Knox, J. B. Cross, V. Bakken, C. Adamo, J. Jaramillo, R. Gomperts, R. E. Stratmann, O. Yazyev, A. J. Austin, R. Cammi, C. Pomelli, J. W. Ochterski, R. L. Martin, K. Morokuma, V. G. Zakrzewski, G. A. Voth, P. Salvador, J. J. Dannenberg, S. Dapprich, A. D. Daniels, O. Farkas, J. B. Foresman, J. V. Ortiz, J. Cioslowski and D. J. Fox, *GAUSSIAN 16, Revision A.03*, Gaussian Inc., Wallingford, Conn, USA, 2015.
36 Y. Shao, L. F. Molnar, Y. Jung, J. Kussmann, C. Ochsenfeld, S. T. Brown, A. T. B. Gilbert, L. V. Slipchenko, S. V. Levchenko, D. P. O'Neill, R. A. DiStasio Jr., R. C. Lochan, T. Wang, G. J. O. Beran, N. A. Besley, J. M. Herbert, C. Y. Lin, T. Van Voorhis, S. H. Chien, A. Sodt, R. P. Steele, V. A. Rassolov, P. E. Maslen, P. P. Korambath, R. D. Adamson, B. Austin, J. Baker, E. F. C. Byrd, H. Dachsel, R. J. Doerksen, A. Dreuw, B. D. Dunietz, A. D. Dutoi, T. R. Furlani, S. R. Gwaltney, A. Heyden, S. Hirata, C.-P. Hsu, G. Kedziora, R. Z. Khalliulin, P. Klunzinger, A. M. Lee, M. S. Lee, W. Z. Liang, I. Lotan, N. Nair, B. Peters, E. I. Proynov, P. A. Pieniazek, Y. M. Rhee, J. Ritchie, E. Rosta, C. D. Sherrill, A. C. Simmonett, J. E. Subotnik, H. L. Woodcock III, W. Zhang, A. T. Bell, A. K. Chakraborty, D. M. Chipman, F. J. Keil, A. Warshel, W. J. Hehre, H. F. Schaefer, J. Kong, A. I. Krylov, P. M. W. Gill and M. Head-Gordon, *Phys. Chem. Chem. Phys.*, 2006, **8**, 3172–3191.
37 C. J. Cramer and D. G. Truhlar, *Chem. Rev.*, 1999, **99**, 2161–2200.
38 M. J. Kamlet, J. L. M. Abboud, M. H. Abraham and R. W. Taft, *J. Org. Chem.*, 1983, **48**, 2877–2887.
39 J. H. Jensen, *Molecular Modeling Basics*, CRC Press, Taylor and Francis, NY, 2010, ch. 3, p. 95.
40 E. Bakeir, G. M. Attia, M. Lukyanova, B. Lukyanov and M. S. A. Abdel-Mottaleb, *Res. Lett. Phys. Chem.*, 2008, **2008**, 314898.
41 R. G. Parr and W. Yang, *J. Am. Chem. Soc.*, 1984, **106**, 4049–4050.
42 C.-Y. Lee, C.-H. Hu, S.-L. Cheng, C.-C. Chu and V. K. S. Hsiao, *J. Lumin.*, 2015, **159**, 246–250.

